Region-wide synchrony and traveling waves of dengue across eight countries in Southeast Asia

Willem G. van Panhuis[a,1], Marc Choisy[b,c], Xin Xiong[a], Nian Shong Chok[a], Pasakorn Akarasewi[d], Sopon Iamsirithaworn[d], Sai K. Lam[e], Chee K. Chong[f], Fook C. Lam[g], Bounlay Phommasak[h], Phengta Vongphrachanh[i], Khamphaphongphane Bouaphanh[i], Huy Rekol[j], Nguyen Tran Hien[k], Pham Quang Thai[k], Tran Nhu Duong[k], Jen-Hsiang Chuang[l], Yu-Lun Liu[l], Lee-Ching Ng[m], Yuan Shi[m], Enrique A. Tayag[n], Vito G. Roque Jr.[n], Lyndon L. Lee Suy[o], Richard G. Jarman[p], Robert V. Gibbons[q], John Mark S. Velasco[q], In-Kyu Yoon[r], Donald S. Burke[a], and Derek A. T. Cummings[s,t]

[a]Department of Epidemiology, University of Pittsburgh Graduate School of Public Health, Pittsburgh, PA 15261; [b]Laboratoire Maladies Infectieuses et Vecteurs Écologie, Génétique, Évolution et Controle, Unité Mixte de Recherche 224 Centre National de la Recherche Scientifique-Institut de Recherche pour le Développement-Université de Montpellier, Institut de Recherche pour le Développement Montpellier, 34394 Montpellier, France; [c]Oxford University Clinical Research Unit, Wellcome Trust Major Overseas Programme, National Hospital for Tropical Diseases, Hanoi 100000, Vietnam; [d]Bureau of Epidemiology, Thailand Ministry of Public Health, Bangkok 10220, Thailand; [e]High Impact Research, University of Malaya, 50603 Kuala Lumpur, Malaysia; [f]Disease Control Division, Malaysia Ministry of Health, 62590 Putrajaya, Malaysia; [g]Western Sussex Hospitals National Health Service Trust, Worthing Hospital, West Sussex BN11 2DH, United Kingdom; [h]Department of Communicable Disease Control, Ministry of Health, Vientiane 0100, Lao People's Democratic Republic; [i]National Center for Laboratory and Epidemiology, Ministry of Health, Vientiane 0100, Lao People's Democratic Republic; [j]National Dengue Control Program, Cambodia Ministry of Health, Phnom Penh 12000, Cambodia; [k]Department of Epidemiology, Vietnam National Institute of Hygiene and Epidemiology, Hanoi 100000, Vietnam; [l]Centers for Disease Control, Taiwan Ministry of Health and Welfare, Taipei City 10050, Taiwan; [m]Environmental Health Institute, Singapore National Environment Agency, Singapore 228231; [n]National Epidemiology Center, Philippines Department of Health, Manila 1003, Philippines; [o]National Center for Disease Prevention and Control, Philippines Department of Health, Manila 1003, Philippines; [p]Viral Disease Branch, Walter Reed Army Institute of Research, Silver Spring, MD 20910; [q]Department of Virology, US Armed Forces Research Institute of Medical Sciences, Bangkok 10400, Thailand; [r]Dengue Vaccine Initiative, International Vaccine Institute, Seoul, 08826 Korea; [s]Department of Biology, University of Florida, Gainesville, FL 32610; and [t]Emerging Pathogens Institute, University of Florida, Gainesville, FL 32610

Edited by Rino Rappuoli, GSK Vaccines, Siena, Italy, and approved August 25, 2015 (received for review January 21, 2015)

MEDICAL SCIENCES

Dengue is a mosquito-transmitted virus infection that causes epidemics of febrile illness and hemorrhagic fever across the tropics and subtropics worldwide. Annual epidemics are commonly observed, but there is substantial spatiotemporal heterogeneity in intensity. A better understanding of this heterogeneity in dengue transmission could lead to improved epidemic prediction and disease control. Time series decomposition methods enable the isolation and study of temporal epidemic dynamics with a specific periodicity (e.g., annual cycles related to climatic drivers and multiannual cycles caused by dynamics in population immunity). We collected and analyzed up to 18 y of monthly dengue surveillance reports on a total of 3.5 million reported dengue cases from 273 provinces in eight countries in Southeast Asia, covering ∼10^7 km^2. We detected strong patterns of synchronous dengue transmission across the entire region, most markedly during a period of high incidence in 1997–1998, which was followed by a period of extremely low incidence in 2001–2002. This synchrony in dengue incidence coincided with elevated temperatures throughout the region in 1997–1998 and the strongest El Niño episode of the century. Multiannual dengue cycles (2–5 y) were highly coherent with the Oceanic Niño Index, and synchrony of these cycles increased with temperature. We also detected localized traveling waves of multiannual dengue epidemic cycles in Thailand, Laos, and the Philippines that were dependent on temperature. This study reveals forcing mechanisms that drive synchronization of dengue epidemics on a continental scale across Southeast Asia.

dengue | epidemiology | surveillance data | Southeast Asia | dynamics

Dengue virus (DENV) is an arbovirus transmitted by *Aedes* mosquitos in the tropics and subtropics of the world. The virus causes an estimated 390 million infections per year, resulting in 96 million clinically symptomatic cases (1). DENV has four serotypes (DENV-1, DENV-2, DENV-3, and DENV-4) that each circulate worldwide. The spatial propagation of dengue transmission at short distances by the mosquito vector is well-understood, but the mechanism of long-distance spread has remained unclear. Disease transmission over large geographical distances is difficult to measure directly, but epidemiological coupling of locations revealed by synchrony in population-level disease patterns has been used successfully in the past to infer mechanisms of spread (2–4). For example, synchrony and its spatial hierarchies indicated that measles in the United Kingdom spread from urban centers to rural areas through a mechanism of fadeout and reintroduction (2). Other studies have suggested that influenza in the United States spreads through workforce commuting (3) and that dengue spreads along a major road in Cambodia (5). Studying epidemic synchrony requires data at high spatiotemporal resolution for a large sample of locations. Data limitations have restricted previous studies on disease spread and synchrony to small geographical areas within country boundaries. Given the increased (cross-border) mobility of populations, strong evidence of global warming, and potential for rapid, global spread of highly pathogenic infectious diseases, a better understanding of the mechanisms of

Significance

Persons living in the tropics and subtropics are at risk for dengue fever and dengue hemorrhagic fever, and large epidemics occur unexpectedly that can overburden healthcare systems. The spatial and temporal dynamics of dengue transmission are poorly understood, limiting disease control efforts. We compiled a large-scale dataset and analyzed continental-scale patterns of dengue in Southeast Asia. Our analysis shows that periods of elevated temperatures can drive the occurrence of synchronous dengue epidemics across the region. This multicountry collaborative study improved insight that may lead to improved prediction of dengue transmission patterns and more effective disease surveillance and control efforts.

Author contributions: W.G.v.P., M.C., D.S.B., and D.A.T.C. designed research; W.G.v.P., M.C., X.X., N.S.C., P.A., S.I., S.K.L., C.K.C., F.C.L., B.P., P.V., K.B., H.R., N.T.H., P.Q.T., T.N.D., J.-H.C., Y.-L.L., L.-C.N., Y.S., E.A.T., V.G.R., L.L.L.S., R.G.J., R.V.G., J.M.S.V., I.-K.Y., D.S.B., and D.A.T.C. performed research; W.G.v.P., M.C., X.X., N.S.C., and D.A.T.C. analyzed data; and W.G.v.P., M.C., S.I., S.K.L., F.C.L., K.B., H.R., P.Q.T., Y.-L.L., R.G.J., R.V.G., D.S.B., and D.A.T.C. wrote the paper.

The authors declare no conflict of interest.

This article is a PNAS Direct Submission.

[1]To whom correspondence should be addressed. Email: wav10@pitt.edu.

This article contains supporting information online at www.pnas.org/lookup/suppl/doi:10.1073/pnas.1501375112/-/DCSupplemental.

long-distance disease spread and spatial synchrony is becoming essential for global health security.

Some infectious diseases in endemic settings, such as dengue or influenza, occur annually in well-defined cycles that depend on climate factors, such as precipitation. In addition to an annual cycle, significant variability at multiannual periodicities has been observed for dengue (6, 7). This multiannual periodicity is thought to be driven by cycling of immunity in the host population and has been observed to vary over time (6). To better understand the spatiotemporal dynamics of large epidemics, previous studies used various time series decomposition methods to isolate multiannual oscillations from background annual cycles and higher frequency noise. For example, previous work on disease spread focused on the 1.5–3 y cycle for measles (2), the 3.5–4.5 and 5–6 y cycles for pertussis (8), and the 2–3 y (9, 10) and 3–4 y cycles (6) for dengue.

Whereas mechanisms that cause spatial patterns of multiannual cycles of diseases, such as measles and pertussis, are known (2, 4, 11), these mechanisms remain unclear for dengue. Previous studies have suggested that immunity-driven extinction–reintroduction dynamics of DENV serotypes can play a role, particularly around urban centers (6, 12). The role of multiyear climate variation has also been studied but without consistent results (13).

We studied the synchrony of multiannual dengue cycles across a large geographical area of eight countries in Southeast Asia that span 3,500 km east to west by 2,500 km north to south, with a combined population of 320 million in 2010. We used monthly dengue surveillance data that represent ∼3.5 million reported cases at the provincial level. High dengue transmission rates across all countries combined with extensive diversity in population density, climate, and geology make this region ideal to investigate the long-distance spread of major dengue epidemics that occurred in this region during the past decades.

Results

Strong Region-Wide Synchrony of Dengue Transmission. We found strong synchrony across the entire region of multiannual dengue cycles and also, for annual cycles and unfiltered incidence rates (IRs) (Figs. 1*A* and 2). The average power (amplitude) of statistically significant multiannual cycles changed over time and was the highest in 1993–2004 (Fig. S1*A*). In comparison, the average power of annual cycles was more constant over time but reduced in 1997–2001 (Fig. S1*B*). We found few statistically significant multiannual cycles in the northern provinces and few annual cycles in the north and the south. Temperatures were too low in the north and too constant in the equatorial south to support cyclical dengue transmission. Synchrony of multiannual cycles changed over time, with the strongest median synchrony of 0.59 (interquartile range = 0.48–0.76) in the 1996–2000 time window (Fig. 3). In comparison, the regional median for annual cycles was consistent over time, ranging between 0.50 and 0.64. The median synchrony of the unfiltered IRs fell between that for the annual and multiannual cycles. Using the average wavelet coherency of dengue cycles as an alternative metric for synchrony over time, we found equivalent patterns (Fig. S1 *C* and *D*). Using the entire time series, the average synchrony decreased as the distance between province pairs increased up to ∼1,000 km. (Fig. S2). Synchrony of multiannual cycles peaked at 0.55 [95% confidence interval (95% CI) = 0.45–0.67] compared with annual cycles at 0.70 (95% CI = 0.64–0.75) at short distances.

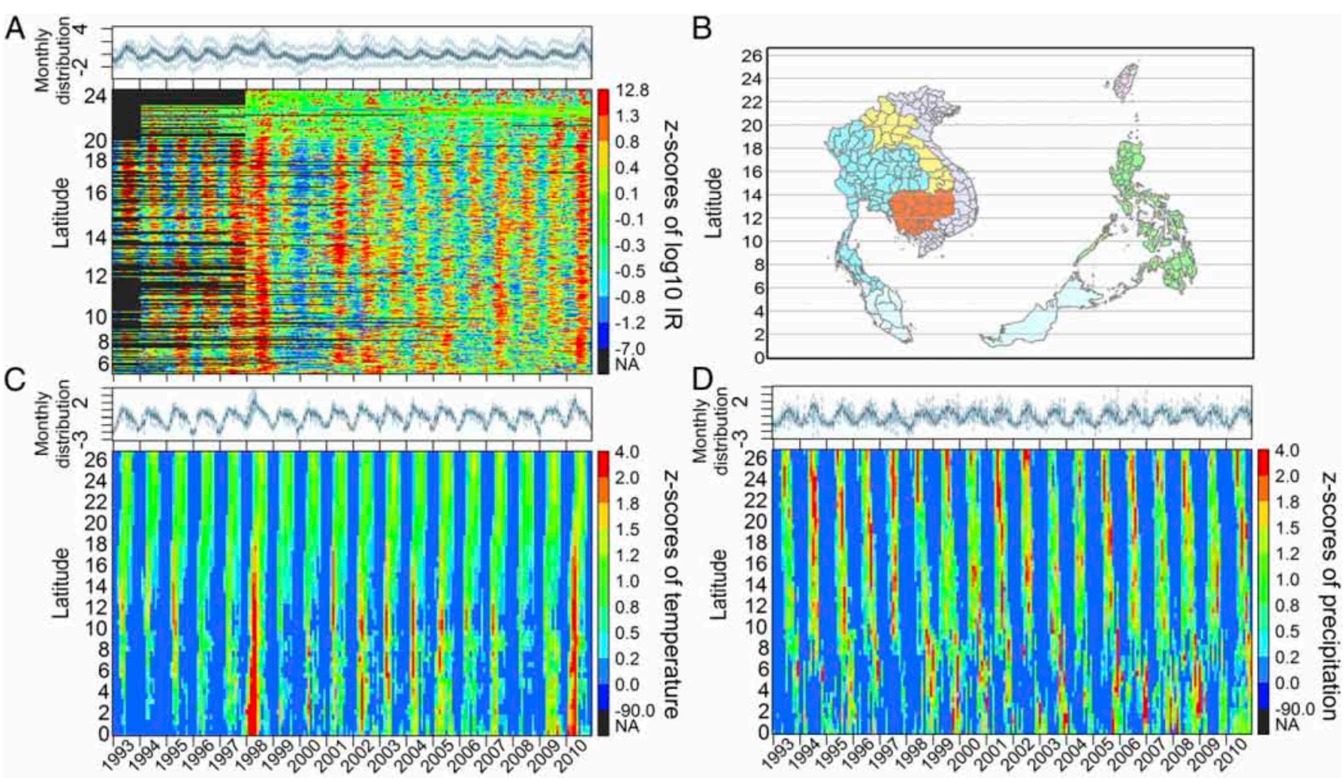

Fig. 1. Monthly dengue IRs (per 100,000 people) and longitudinal climate indicators. Monthly dengue IRs for each province ranked by latitude and monthly climate indicators for corresponding latitudes and time periods. *Upper* shows median values across provinces or latitudes. NA, not available. (*A*) Monthly dengue IRs per 100,000 people that have been centered and reduced into *z* scores, log_{10}-transformed, detrended, and imputed. We imputed missing data by random draws from values of the same months but for different years (Fig. S3). (*B*) Map of the study provinces by latitude. (*C*) Average monthly temperature in degrees Celsius from gridded data covering the entire region averaged by latitude and centered and reduced into *z* scores. (*D*) The same as *C* but for total monthly precipitation (millimeters).

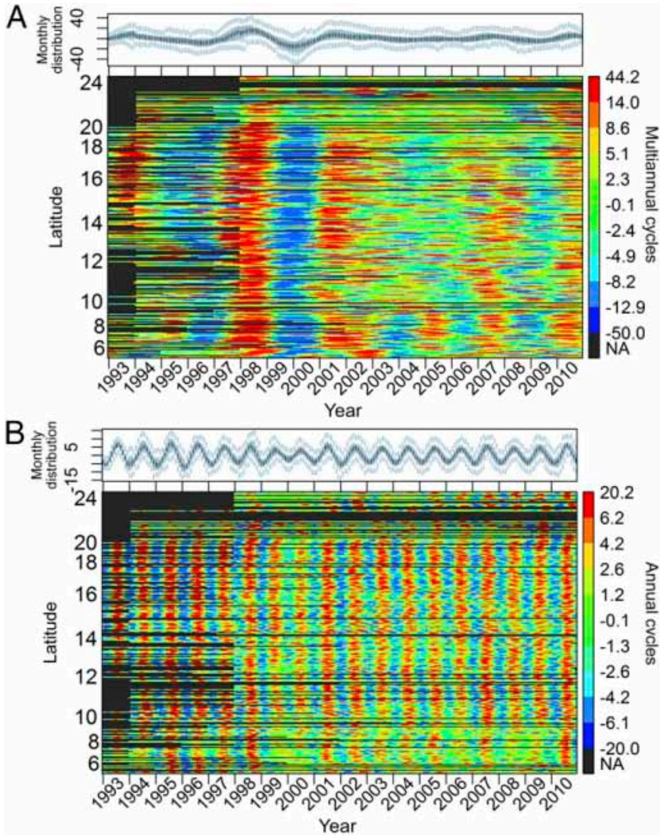

Fig. 2. Wavelet transforms. Reconstructed periodic cycles of monthly dengue IRs for provinces ranked by latitude. *Upper* shows monthly distributions across provinces. NA, not available. (*A*) Reconstructed multiannual cycles. (*B*) Reconstructed annual cycles.

Climate Forcing of Synchrony. The strong synchronization of multiannual dengue cycles in 1997–2001 coincided with high temperatures across most latitudes (Fig. 1*C*) but not with an anomaly in precipitation (Fig. 1*D*). High temperatures in these years were related to the strongest El Niño episode of the past century (14, 15). We measured a strong wavelet coherency (>0.8) between multiannual dengue cycles and the Oceanic Niño Index (ONI) during 1993–2002 and during 2009–2010 for almost all provinces (Fig. 4). Wavelet coherency for the latter period should be interpreted with caution, because it is at the end of the time series and subject to edge effects. Synchrony of multiannual dengue cycles in the 1997–2001 time window was reduced in a corridor running from Laos to eastern Cambodia (Fig. 3*B* and Fig. S4*A*). This area is characterized by high altitude and low temperatures and includes the Annamite Mountain Range (Fig. S4). When studying synchrony between each of 12 major cities in the region and all other provinces, we found two clusters of cities: one cluster consisting of Bangkok, Singapore, Zamboanga (the Philippines), Davao, Cebu, and Taipei, that was synchronous with the Annamite corridor, and a second cluster consisting of Phnom Penh, Vientiane, Hanoi, and Kuala Lumpur, that was synchronous with the Annamite corridor (Fig. S4). These clusters of different synchrony suggest at least two separate networks of epidemiologically connected areas in this region, possibly determined by temperature. Indeed, using a linear regression, we found that synchrony of multiannual cycles was stronger at higher temperatures: synchrony increased with 0.029 for each 1 °C increase in temperature (95% CI = 0.026–0.031) (Table S1). For annual cycles, this coefficient was much lower at 0.004 (95% CI = 0.002–0.005). These results suggest that temperature plays a significant role in the spread of major dengue epidemics. Interestingly, we also found a negative association between population density and synchrony for both annual ($\beta = -0.088/\log_{10}$ population density per km^2) and multiannual ($\beta = -0.037/\log_{10}$ population density per km^2) cycles. This association suggests that more densely populated areas may be able to determine their own nonsynchronous dynamics as independent "pacemakers" instead of phase-locking dynamics with other areas.

Traveling Waves of Multiannual Cycles. We detected traveling waves of multiannual dengue cycles in various parts of the region. We used the phase difference θ to determine the difference (in months) in epidemic timing between provinces. A province could have either a positive- or negative θ compared with another province. A positive θ indicated that a province was timed earlier (leading ahead) vs. the other, and a negative θ indicated that a province was timed later (lagging behind). Outgoing traveling waves can emerge from a province with epidemic dynamics timed ahead of others. In contrast, a province with epidemics lagging behind others could experience an incoming traveling wave. For each province separately, we tested for the presence of local incoming or outgoing traveling waves. For provinces that were lagging behind ($\theta < 0$), we defined an incoming traveling wave as a decreasing lag time with decreasing distance. For provinces that were leading ahead ($\theta > 0$), we defined an outgoing traveling wave as an increasing lag time with increasing distance; 28 provinces had statistically significant incoming traveling waves of multiannual dengue cycles, and 33 had outgoing traveling waves (Fig. 5). Provinces with outgoing traveling waves were located in west Thailand and the Bangkok area, central Laos (Savannakhét and Khammouan), and southern Philippines (Bohol). We found fewer incoming traveling waves for annual cycles concentrated in the northern Philippines ($n = 8$) and central-eastern Thailand ($n = 21$). The presence of multiannual waves but not annual waves was statistically significantly associated with temperature and precipitation. Provinces with outgoing multiannual waves had an average of 1.5 °C higher temperature (95% CI = 1.0–2.1 °C) and 53.1 mm (95% CI = 39.7–66.6 mm) lower precipitation compared to provinces without waves. Provinces with incoming multiannual waves had an average of 39.5 mm (95% CI = 22.4–56.5 mm) lower precipitation, but no significant temperature difference compared to other provinces.

Discussion

This analysis of large-scale surveillance data revealed strong region-wide synchrony in multiannual dengue cycles. We used a "synoptic epidemiology" approach that spans a large geographical scale but includes granular detail, providing an instantaneous picture of region-wide and local disease dynamics. Synchrony of multiannual cycles changed over time, with a maximal region-wide synchronization occurring during 1997–2001, whereas synchrony of the annual cycles was consistent over time. Synchrony of multiannual dengue cycles during this period coincided with the highest temperatures of the study period across most latitudes and the strongest El Niño event of the century (14, 15). We measured strong wavelet coherency between multiannual dengue cycles and the ONI across most provinces during 1993–2002, but this coherency decreased afterward. A previous study found identical nonstationary wavelet coherency during this period between multiannual dengue cycles and El Niño Southern Oscillation indices for one province in Vietnam (Binh Thuan) (9). The transient nature of this association over time suggests a threshold effect, where the spread of major DENV epidemics may be facilitated by abnormally high temperatures or high temperatures for an abnormally long period. Indeed, we found that synchrony of multiannual cycles increased as temperature increased. Throughout 1997 and 1998, high temperatures across the region could have sustained high levels of dengue transmission, leading to a depletion of susceptibles and low transmission in the following years (Fig. 1*A*). This hypothesis is consistent

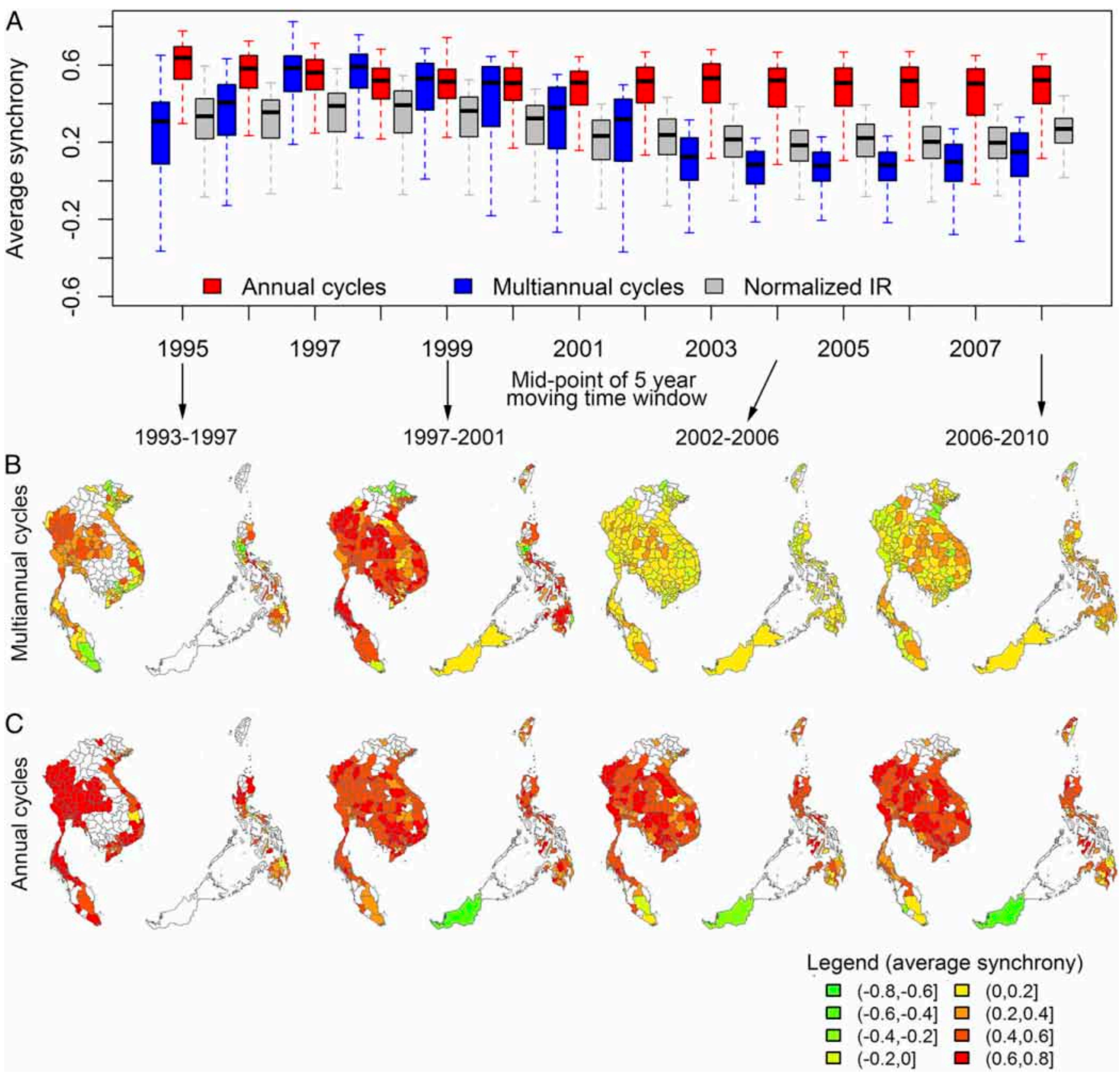

Fig. 3. Synchrony of dengue cycles over time. We computed the average synchrony for moving, overlapping 5-y windows to detect changes over time. (*A*) Distributions of average synchrony per province per time window plotted at the midyear of each window for multiannual and annual cycles and unfiltered IRs. (*B*) The average synchrony of multiannual dengue cycles per province for four time windows. (*C*) The same as *B* but for annual cycles.

with the biology of the *Aedes aegypti* vector, which reproduces faster and transmits DENV more efficiently at higher temperatures (16, 17). Also, in 1998, a new DENV-2 strain (Cosmopolitan genotype) emerged in Asia (18). High temperatures across a sufficiently large geographical area combined with a large pool of susceptibles could enable the spread of major synchronous dengue epidemics when new DENV types emerge. Indeed, we found a 1.5 °C higher temperature in provinces with outgoing multiannual traveling waves compared to provinces without these waves.

Synchrony of multiannual as well as annual cycles was inversely associated with population density. This association could suggest an extinction–reinvasion mechanism, where synchronous cycles emerge in areas of low population density after a period of low transmission. Densely populated areas are less prone to such "fade-outs," because they supply a constant pool of susceptibles that can sustain ongoing transmission of all four DENV serotypes. These urban centers could act as independent pacemakers of epidemic dengue cycles into the surrounding areas (6, 12). This mechanism is consistent with the two clusters of synchrony among major cities in the region: one synchronous with the Annamite Mountain Range and the other synchronous with the west-central Thailand area. These areas are also the two main areas for which we detected outgoing traveling waves for multiannual cycles, suggesting that forcing mechanisms, such as temperature, act independently in each of these areas.

The role of human movement in the spread of disease epidemics has been a strong focus of recent research, greatly facilitated by the emergence of novel data sources, such as mobile phone and flight

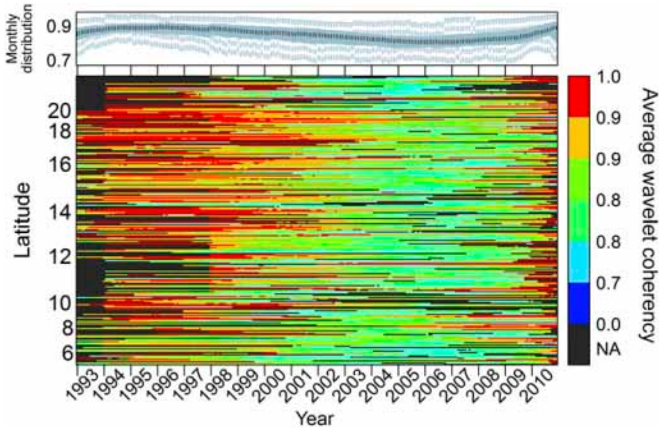

Fig. 4. Wavelet coherency between the ONI and multiannual DENV cycles. The monthly average statistically significant wavelet coherency between ONI and multiannual DENV cycles across (*Lower*) the multiannual periodicity band for each province ranked by latitude. *Upper* shows the distributions (medians and interquartile ranges) of province average wavelet coherency per month. NA, not available.

data (19, 20). Strong synchrony and traveling waves of dengue epidemics across Southeast Asia could be driven by (cross-border) population movement. We were unable to formally test this because of limited data on human movement. However, a high degree of population connectivity and spread of DENV across country borders in Southeast Asia has been shown by phylogenetic studies, showing that DENV genotypes circulating in countries, such as Thailand and the Philippines, were isolated across the entire region (18, 21–23). We found spatial structuring in time lags of dengue cycles across provinces that was consistent with traveling waves of dengue incidence. Outgoing traveling waves were concentrated in central Thailand, the east Mekong, and the southern Philippines. It was also in these countries that dengue was first recognized in the 1950s (24). Provinces with outgoing traveling waves had higher temperatures and lower precipitation compared to other provinces. Local climate, virus, and population conditions in these areas may have ignited the emergence and spread of new DENV types that resulted in region-wide synchronous dynamics through widespread high temperatures during a strong El Niño episode and population movement.

Powerful forcing mechanisms in Southeast Asia, particularly sustained high temperatures, can drive the synchronized spread of major dengue epidemics on a continental scale. This analysis improves opportunities for future studies on the causal mechanisms and for predictive modeling of large-scale dynamics of dengue as well as other infectious diseases. This study also demonstrates the advantages of multicountry collaboration to advance infectious disease surveillance, analysis, and control.

Materials and Methods

Data. Monthly dengue surveillance data and corresponding population (25) and climate data (26–28) at the provincial level (29) were available for 273 provinces in Thailand, Cambodia, Laos, Vietnam, Malaysia, Singapore, the Philippines, and Taiwan (more details on data sources and inclusion are in *SI Materials and Methods*). We computed monthly dengue IRs per 100,000 people for 1993–2010 for provinces in Thailand, Malaysia, and Singapore; 1994–2010 for the Philippines and Vietnam; and 1998–2010 for the other countries (Figs. S3 and S5 and Movie S1). All data are publicly available through Project Tycho (www.tycho.pitt.edu).

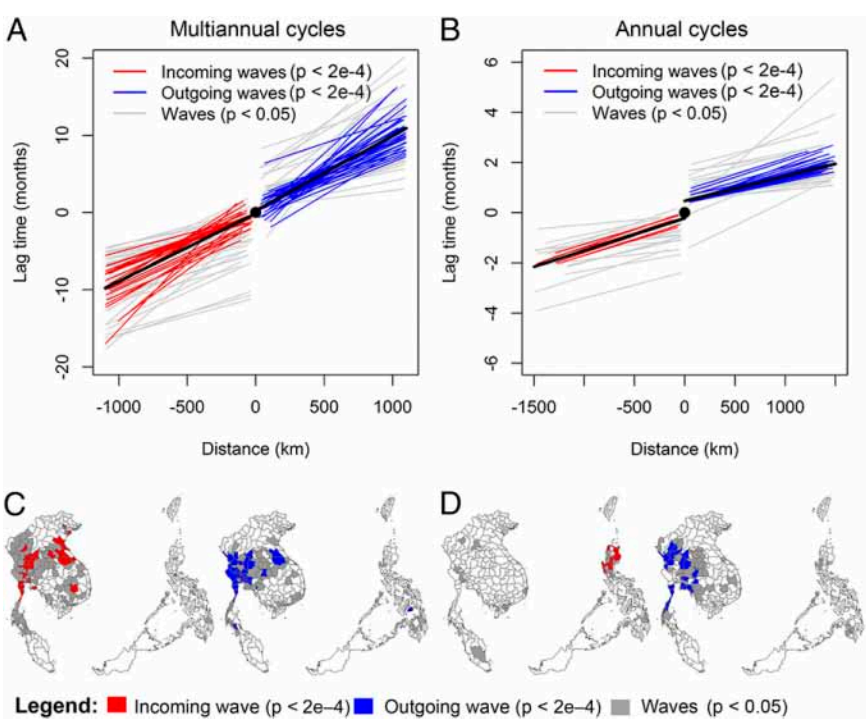

Fig. 5. Traveling waves of synchrony across provinces. For each province, we fitted a linear model of the phase difference θ of multiannual and annual dengue cycles vs. geographical distance (kilometers). A negative θ indicated that a province epidemic cycle was timed later than another province, possibly experiencing an incoming traveling wave (decreasing θ with decreasing distance). A positive θ indicated that a province was timed earlier than another province, possibly experiencing a positive traveling wave (increasing θ with increasing distance). For $\theta < 0$, we inversed the distance for more intuitive displays. (*A*) Fitted values of linear models of θ for multiannual cycles vs. distance for each province. We fitted models separately for incoming and outgoing waves. Fitted values are only shown for provinces with a statistically significant model coefficient. We used a Bonferroni-corrected significance level ($P < 2e{-}4$) for each province but also, showed fitted values for models with significant coefficients at the 0.05 level (gray lines). The fitted values for the regional average model are shown as black lines. (*B*) The same as *A* but for annual cycles. (*C*) Provinces with statistically significant incoming (red) and outgoing (blue) waves of multiannual cycles. (*D*) The same as *C* but for annual cycles.

Wavelet Transforms. We used wavelet methods to decompose reported dengue IRs into multiannual and annual cycles as described previously (2, 8, 9, 30, 31). Wavelet transforms are appropriate to characterize nonstationary signals with multiple periodicities, such as dengue IRs (6). We used a Morlet wavelet with a nondimensional frequency $\omega_0 = 6$ as used previously (8, 30). This wavelet is complex, enabling the extraction of phase angles to study epidemic timing. We explored the influence of the selected value of ω_0 on synchrony in a sensitivity analysis and found that only extreme values influenced study results (Fig. S6). We found that most provinces had statistically significant annual cycles with a periodicity of 6–18 mo and statistically significant multiannual cycles with a periodicity of 19–60 mo (Fig. S7). We analyzed reconstructions of these cycles for provinces with statistically significant cycles in the annual or multiannual periodicity range.

Synchrony. We used pairwise Pearson correlation coefficients of multiannual and annual dengue cycles and unfiltered IRs between provinces to measure synchrony ρ. Pearson correlation indicates similarity in both timing and amplitude of epidemic cycles. We computed the average ρ for a province as the average across all province pairs that included that province weighted by the number of pairs with non-missing data. We computed this average using the entire time series of dengue cycles but also, for moving, overlapping 5-y time windows. We also computed the average wavelet coherency between province pairs in the annual and multiannual periodicity bands as described previously (7, 32) using parameter values for the wavelet transforms as described. Wavelet coherency (ranging from zero to one) describes the phase relationship between two time series localized in a time–periodicity spectrum. For strong wavelet coherency, statistically significant cycles of a specific periodicity need to be phase-locked (positively or negatively). We also used wavelet coherency to assess the association between multiannual dengue cycles and the ONI. The ONI identifies El Niño and La Niña events in the tropical Pacific based on sea surface temperature in the Niño 3.4 Region. To measure the dependency of synchrony on the average level of population density, temperature, and precipitation of province pairs, we used a multivariate linear regression with synchrony as the dependent variable and these covariates as independent variables.

Phase Angles. We used phase angle transforms of multiannual and annual cycles to study epidemic timing as described previously (2, 7, 31, 32). We expressed the pairwise phase difference θ between province pairs in months by assuming a 12-mo periodicity for annual cycles and 39-mo periodicity for multiannual cycles. We defined a traveling wave for a province as a statistically significantly linear association between θ and geographical distances for that province vs. all others (Fig. S8). A negative θ indicated that a province epidemic cycle was timed later vs. others and that this province could have an incoming traveling wave. A positive θ indicated that a province was timed earlier and could have an outgoing wave. For each province, we tested the presence of "local" incoming traveling waves (decreasing θ with decreasing distance for $\theta < 0$) and local outgoing traveling waves (increasing θ with increasing distance for $\theta > 0$) using a linear regression model:

$$\theta_{p,q} = \begin{cases} C - \beta_p d_{p,q} & \text{for } \theta < 0, \text{ incoming waves} \\ C + \beta_p d_{p,q} & \text{for } \theta > 0, \text{ outgoing waves} \end{cases},$$

where $\theta_{p,q}$ is the lag time between provinces p and q for annual or multiannual cycles, and $d_{p,q}$ is the distance in kilometers between provinces. We inversed the sign of distance for negative lag times for more intuitive displays of incoming waves. We defined local as distances ≤1,000 km (multiannual cycles) or ≤1,500 km (annual cycles). Using a linear model of θ vs. distance including all province pairs, we found that, after these distances, θ did not continue to statistically significantly change with distance. We defined a statistically significant traveling wave as a positive β_p using a Bonferroni-corrected significance level of 2e–4 for each province, resulting in a combined level of 0.05 across all provinces. We used a logistic regression to estimate the role of population size, temperature, and precipitation (independent variables) on the occurrence of traveling waves (dependent binary variable).

The entire analysis was conducted in the R Statistical Package, version 3.2.1.

ACKNOWLEDGMENTS. The authors thank surveillance data managers in each country for support in compiling dengue surveillance data. We also thank Dr. Nyphonh (Lao People's Democratic Republic), Ms. Hannah Lewis (WHO), Dr. Torréton (Institut de Recherche pour le Développement, Vietnam), and Dr. Sok Touch (CDC Cambodia) for support in facilitating collaborations and Mr. Guido Camargo for proofreading of this manuscript. W.G.v.P., D.A.T.C., X.X., N.S.C., M.C., and D.S.B. would like to thank the Bill and Melinda Gates Foundation (Grant 49276, Evaluation of Candidate Vaccine Technologies Using Computational Models) and the US National Institute of General Medical Sciences (Grant 5U54GM088491, Computational Models of Infectious Disease Threats) for their support. S.K.L. would like to thank the University of Malaya for their support (UM.C/HIR/MOHE/CHAN/15). M.C. would like to thank the Groupe de Recherche International (GDRI) "Biodiversity and infectious diseases in Southeast Asia." D.A.T.C. was funded by a Career Award at the Scientific Interface from the Burroughs Wellcome Fund and the US NIH R01AI102939 and R01AI114703.

1. Bhatt S, et al. (2013) The global distribution and burden of dengue. *Nature* 496(7446): 504–507.
2. Grenfell BT, Bjørnstad ON, Kappey J (2001) Travelling waves and spatial hierarchies in measles epidemics. *Nature* 414(6865):716–723.
3. Viboud C, et al. (2006) Synchrony, waves, and spatial hierarchies in the spread of influenza. *Science* 312(5772):447–451.
4. Rohani P, Earn DJ, Grenfell BT (1999) Opposite patterns of synchrony in sympatric disease metapopulations. *Science* 286(5441):968–971.
5. Teurlai M, et al. (2012) Can human movements explain heterogeneous propagation of dengue fever in Cambodia? *PLoS Negl Trop Dis* 61(12):e1957.
6. Cummings DAT, et al. (2004) Travelling waves in the occurrence of dengue haemorrhagic fever in Thailand. *Nature* 427(6972):344–347.
7. Cazelles B, Chavez M, Magny GC, Guégan J-F, Hales S (2007) Time-dependent spectral analysis of epidemiological time-series with wavelets. *J R Soc Interface* 4(15):625–636.
8. Choisy M, Rohani P (2012) Changing spatial epidemiology of pertussis in continental USA. *Proc Biol Sci* 279(1747):4574–4581.
9. Thai KTD, et al. (2010) Dengue dynamics in Binh Thuan province, southern Vietnam: Periodicity, synchronicity and climate variability. *PLoS Negl Trop Dis* 4(7):e747.
10. Cuong HQ, et al. (2011) Quantifying the emergence of dengue in Hanoi, Vietnam: 1998-2009. *PLoS Negl Trop Dis* 5(9):e1322.
11. Magpantay FMG, Rohani P (2015) Dynamics of pertussis transmission in the United States. *Am J Epidemiol* 181(12):921–931.
12. Gubler DJ (2004) Cities spawn epidemic dengue viruses. *Nat Med* 10(2):129–130.
13. Johansson MA, Cummings DA, Glass GE (2009) Multiyear climate variability and dengue–El Niño southern oscillation, weather, and dengue incidence in Puerto Rico, Mexico, and Thailand: A longitudinal data analysis. *PLoS Med* 6(11):e1000168.
14. Slingo JM, Annamalai H (2000) 1997: The El Niño of the century and the response of the Indian summer monsoon. *Mon Weather Rev* 128(6):1778–1797.
15. Webster PJ, Palmer TN (1997) The past and the future of El Niño. *Nature* 390(12):562–564.
16. Watts DM, Burke DS, Harrison BA, Whitmire RE, Nisalak A (1987) Effect of temperature on the vector efficiency of *Aedes aegypti* for dengue 2 virus. *Am J Trop Med Hyg* 36(1):143–152.
17. Brady OJ, et al. (2014) Global temperature constraints on Aedes aegypti and Ae. albopictus persistence and competence for dengue virus transmission. *Parasit Vectors* 7:338.
18. Salda LTD, et al. (2005) Molecular epidemiology of dengue 2 viruses in the Philippines: Genotype shift and local evolution. *Am J Trop Med Hyg* 73(4):796–802.
19. Wesolowski A, O'Meara WP, Eagle N, Tatem AJ, Buckee CO (2015) Evaluating spatial interaction models for regional mobility in Sub-Saharan Africa. *PLOS Comput Biol* 11(7):e1004267.
20. Colizza V, Barrat A, Barthélemy M, Vespignani A (2006) The role of the airline transportation network in the prediction and predictability of global epidemics. *Proc Natl Acad Sci USA* 103(7):2015–2020.
21. Vu TTH, et al. (2010) Emergence of the Asian 1 genotype of dengue virus serotype 2 in viet nam: In vivo fitness advantage and lineage replacement in South-East Asia. *PLoS Negl Trop Dis* 4(7):e757.
22. Holmes EC, Tio P-H, Perera D, Muhi J, Cardosa J (2009) Importation and co-circulation of multiple serotypes of dengue virus in Sarawak, Malaysia. *Virus Res* 143(1):1–5.
23. Lee K-S, et al. (2012) Dengue virus surveillance in Singapore reveals high viral diversity through multiple introductions and in situ evolution. *Infect Genet Evol* 12(1):77–85.
24. Hammon WM, Rudnick A, Sather GE (1960) Viruses associated with epidemic hemorrhagic fevers of the Philippines and Thailand. *Science* 131(3407):1102–1103.
25. US Census Bureau (2014) *International Database*. Available at www.census.gov/population/international/data/idb/informationGateway.php. Accessed July 14, 2014.
26. Fan Y, van den Dool H (2008) A global monthly land surface air temperature analysis for 1948–present. *J Geophys Res* 113(D1):D01103.
27. Becker A, et al. (2013) A description of the global land-surface precipitation data products of the Global Precipitation Climatology Centre with sample applications including centennial (trend) analysis from 1901–present. *Earth Syst Sci Data* 5(1):71–99.
28. Center for International Earth Science Information Network (CIESIN), Columbia University; Centro Internacional de Agricultura Tropical (CIAT) (2005) *Gridded Population of the World Version 3 (GPWv3)* [NASA Socioeconomic Data and Applications Center (SEDAC), Palisades, NY].
29. GADM (2013) *Database of Global Administrative Areas.* Available at gadm.org/home. Accessed July 21, 2015.
30. Torrence C, Compo GP (1998) A practical guide to wavelet analysis. *Bull Am Meteorol Soc* 79(1):61–78.
31. Cazelles B, et al. (2008) Wavelet analysis of ecological time series. *Oecologia* 156(2): 287–304.
32. Grinsted A, Moore JC, Jevrejeva S (2004) Application of the cross wavelet transform and wavelet coherence to geophysical time series. *Nonlinear Process Geophys* 11(5/6):561–566.
33. Bjørnstad ON, Falck W (2001) Nonparametric spatial covariance functions: Estimation and testing. *Environ Ecol Stat* 8(1):53–70.

Supporting Information

van Panhuis et al. 10.1073/pnas.1501375112

SI Materials and Methods

1.1. Data Collection. We collected monthly dengue surveillance data at the provincial level for Thailand, Cambodia, Laos, Vietnam, Malaysia, Singapore, the Philippines, and Taiwan. Data for Thailand were provided by the Thai Ministry of Public Health Bureau of Epidemiology (1968–2010). Data for Cambodia were provided by the Cambodia Ministry of Health (MOH) National Dengue Control Program (1998–2009) and supplemented with data from the WHO DengueNet Database (1998–2010) and the WHO Western Pacific Regional Office (1998–2001) where needed. Data for Laos were provided by the Lao People's Democratic Republic MOH National Center for Laboratory and Epidemiology (1998–2010) and supplemented with data from the WHO DengueNet Database (1998–2007) and the WHO Western Pacific Regional Office (1998–2001) where needed. Data for Vietnam were provided by the National Institute of Hygiene and Epidemiology (1994–2010). Data for Malaysia were provided by the Malaysia MOH Disease Control Division (1988–2010). Data for Singapore were provided by the Singapore National Environment Agency (1993–2010). Data for the Philippines were provided by the Philippines MOH National Epidemiology Center (1993–2010), and data for Taiwan were provided by the Taiwan Centers for Disease Control (1998–2010). Dengue surveillance systems were similar across countries and mostly passive, except for the Philippines and Cambodia (sentinel system). In most countries, dengue is predominantly reported among children. Cambodia was the only country for which dengue surveillance was explicitly restricted to children <15 y old. Despite these slight differences, population-level disease patterns were comparable across all countries. For each country, data were collected at the provincial level. We defined a province as the smallest geographical area for which data were available (the first or second administrative level). Where needed, surveillance reports for dengue fever and dengue hemorrhagic fever were combined into the total number of dengue cases. Population counts were obtained for provinces by year for each country. Population counts for Thailand were provided by the Thai Ministry of Public Health Bureau of Epidemiology (1968–2010); population counts for Cambodia were provided by the National Institute of Statistics (1998) and the MOH National Dengue Control Program (2002–2010). Population counts for Laos were obtained from the Laos Statistics Bureau (1995 and 2000–2010). Population counts for Vietnam were provided by the General Statistics Office of Vietnam (1995–2010). Population counts for Malaysia were provided by the Department of Statistics (2000 and 2003–2010). Population counts for Singapore were obtained from the US Census Bureau International Database (25). Population counts for the Philippines were obtained from the Philippines Census Bureau (2000, 2005, and 2010), and population counts for Taiwan were provided by the Taiwan Centers for Disease Control (1998–2010). Administrative boundary files were obtained from the Global Administrative Areas (GADM) Database (29). Monthly gridded (0.5° × 0.5°) average air temperature (26) and total precipitation (27) data from 1993 to 2010 were obtained from the National Oceanic and Atmospheric Administration Earth System Research Laboratory Physical Sciences Division for latitudes between 0° and 26.8° and longitudes between 96.2° and 127.7°. Gridded (2.5 × 2.5 km) data on population density (per kilometer^2) for the year 2000 were obtained from the Center for International Earth Science Information Network at Columbia University (28). Finally, we obtained monthly data on the Oceanic Niño Index (ONI) from the National Oceanic and Atmospheric Administration Center for Weather and Climate Prediction (www.cpc.ncep.noaa.gov/data/indices). The ONI indicates the strength of the El Niño climate variation based on sea surface temperature in the Niño 3.4 region.

1.2. Data Exclusions. Province names were standardized based on the administrative level one or two divisions in the GADM Database as of 2013 (29). Provinces that could not be located were excluded (e.g., because of a split after the last update of the boundary definition files in the GADM Database). The study period was determined separately for each province. No data before 1993 were included because of lack of data for most countries. For each province, the first and last years of a study period were defined by the first and last years with at least six monthly observations. Provinces were excluded if 12 or more consecutive monthly observations were missing, two-thirds or more of all observations were missing, or if the study period was less than 4 y (2.5 cycles of the smallest multiannual period of 19 mo). These in- and exclusions resulted in a total of 273 of 289 provinces included (94%).

1.3. Data Management. For multiple countries, the numbers and names of provinces changed over time because of merging or splitting events. We used province boundaries as in the GADM Database as of 2013; we merged data for provinces that merged and only used data after a splitting event for provinces that had split. Geographical distances between all province pairs were computed using latitude/longitude of province centroids according to the World Geodetic System 1984 Revision Coordinate System. We computed the average air temperature and precipitation per latitude for each month. We centered and reduced the time series for each latitude to z scores around the latitude mean. We also extracted the average value of air temperature, precipitation, and population density for province polygons from the gridded data. Population estimates were not available for the entire study period of each province. We applied country-specific, nationwide annual population growth rates obtained from the US Census Bureau International Database (25) to estimate the provincial-level population for missing years. The growth rate $r_{c,y}$ in country c and year y was computed as

$$r_{c,y} = \frac{N_{c,y}}{N_{c,y-1}}, \tag{S1}$$

where $N_{c,y}$ is the population size in country c in year y. The population size in province p of country c in year y was then computed from

$$N_{p,c,y} = r_{c,y} \times N_{p,c,y-1}. \tag{S2}$$

We used dengue case data and population estimates to compute monthly IRs per 100,000 people for each province.

1.4. Data Transformation. IRs were log-transformed as

$$\log_{10}\left(10^5 \times \frac{I+1}{N}\right), \tag{S3}$$

where I is the incidence (i.e., number of cases), and N is the population size. The log-transformed IRs were then detrended by subtracting fitted values of a linear model from the observed values. The fitted linear model reads

$$\widehat{IR_{p,m}} = C + \beta_p \times m, \quad \text{[S4]}$$

where β_p is the linear regression coefficient, and m is the study month. The detrended IRs for each province (p) and month (m) are thus

$$\widetilde{IR_{p,m}} = IR_{p,m} - \widehat{IR_{p,m}}, \quad \text{[S5]}$$

where m refers to the month and $IR_{p,m}$ refers to the reported IRs for each province and month. After detrending, missing IRs were imputed separately for each province by randomly selecting an observation for the same month but from a different year. Finally, IRs were centered (discounted the mean) and reduced (divided by the SD) to z scores to increase cross-province comparability.

1.5. Reconstructing Annual and Multiannual Cycles. We used wavelet analysis to isolate cycles with multiannual and annual periodicities from the reported IRs. Wavelet analysis is well-suited to characterize epidemiological time series containing cyclical variability with periodicities that change over time (nonstationarity). Wavelet analysis has been used previously to study a wide range of infectious diseases, such as measles, pertussis, and dengue (2, 5, 8, 9, 11, 13). Detailed methods for wavelet analysis have been described previously (30, 31). We computed Morlet wave transforms for each province using a nondimensional frequency $\omega_0 = 6$ and a periodicity step size δj of 0.25 on a linear scale. The Morlet wavelet enables a high resolution of the periodicity scale and is complex, which makes it possible to extract phase angles to represent epidemic timing (7, 30). The Morlet wavelet has been widely used previously for the study of infectious disease IRs (2, 8, 9, 13). The value for ω_0 of 6 has been used previously (8, 30), and a δj of 0.25 gives a detailed resolution of the periodicity scale (1-mo intervals). We conducted a sensitivity analysis to assess the effect of alternative values for ω_0 and δj on the wavelet transforms and resulting synchrony between province pairs. Only extreme values of ω_0 reduced synchrony, and changes in δj had no noticeable effect (Fig. S6).

For each scale s and time interval δt, the continuous wavelet transform of a time series x_k is defined as in the work by Torrence and Campo (30):

$$W_n(s) = \sum_{k=0}^{N-1} x_k \psi^* \frac{(k-n)\delta t}{s} \quad \text{[S6]}$$

where ψ represents the Morlet wavelet function and * the complex conjugate. n represents the time index, ranging from zero to the total number of time points N. We computed wavelet transforms for periodicities (or scales) ranging from 2 to 60 mo. This range contains all periodic cycles previously observed for dengue IRs. Statistical significance of wavelet transforms was tested by comparing the wave signal with a red noise background signal (30, 31).

For each province, we computed the average of wavelet transforms for each periodic intervals over all time points n (global wavelet spectrum) according to the work by Torrence and Campo (30):

$$\overline{W}^2(s) = \frac{1}{N}\sum_{n=0}^{N} |W_n(s)|^2, \quad \text{[S7]}$$

where N represents the number of observations per province. For each province, we only explored periodicity s below the maximum periodicity $s_{max,p}$, to reduce edge effects. We determined the maximum periodicity for each province p, $s_{max,p}$, as the number of monthly observations divided by 2.5.

Similarly, for each province, we also computed the average of statistically significant wavelet transforms per time interval δt across periodicities in the annual (6–18 mo) and multiannual (19–60 mo) band using the scale-averaged wavelet power according to Torrence and Campo (30):

$$\overline{W_n}^2 = \frac{\delta j \delta t}{C_\delta} \sum_{j=j_1}^{j_2} \frac{|W_n(s_j)|^2}{s_j}, \quad \text{[S8]}$$

where s represents the periodicity included, δj represents the scale interval size, and C_δ is a constant for the Morlet wavelet (0.776). We only explored periodicities below the maximum $s_{max,p}$ supported by the length of province time series. We used j ranging from 6 to 18 mo for the average for annual cycles and from 19 to 60 mo for the average for multiannual cycles.

We reconstructed annual epidemic cycles defined as the average of 6–18 mo periodic cycles and multiannual cycles defined as the average of 19–60 mo periodic cycles. We reconstructed these cycles using the filter described in the work by Torrence and Campo (30):

$$x'_n = \frac{\delta j \sqrt{\delta t}}{C_\delta \Psi_0} \sum_{j=j_1}^{j_2} \frac{\Re\{W_n(s_j)\}}{\sqrt{s_j}}, \quad \text{[S9]}$$

where δj was 0.25, C_δ was 0.776 as previously used (30), and values for $j1$ and $j2$ were 6 and 18 mo, respectively, to reconstruct annual cycles and 19 and 60 mo, respectively, for multiannual cycles. We only reconstructed waves for provinces that had statistically significant wavelet transforms for at least 50 time points within the annual or multiannual periodicity bands.

1.6. Estimating Synchrony. We defined synchrony between provinces as the pairwise Pearson correlation coefficient, taking into account both timing and amplitude of the signals. We computed synchrony for both annual and multiannual cycles. To assess the association between synchrony and geographical distance between provinces, we used a previously described nonparametric covariance function that estimates the underlying correlation without assuming any particular shape (2, 33). It uses a smoothing spline (bandwidth of 300 data points) to estimate the curve and bootstrapping (n = 1,000) to estimate confidence limits:

$$\tilde{\rho}(\delta) = \frac{\sum_{i=1}^{n}\sum_{i=1}^{n} K\left(\frac{\delta_{ij}}{h}\right)(\hat{\rho}_{ij})}{\sum_{i=1}^{n}\sum_{i=1}^{n} K\left(\frac{\delta_{ij}}{h}\right)}, \quad \text{[S10]}$$

where K is a kernel function, h is the bandwidth, and $\hat{\rho}_{ij}$ is the autocorrelation matrix.

We measured changes in synchrony over time by computing synchrony separately for parts of the time series within moving and overlapping 5-y time windows. For each time window, we computed the average synchrony per province weighted by the number of province pairs included. We did this for annual and multiannual cycles and the unfiltered IRs (Fig. 3). We used a linear model to estimate the association between synchrony and the pairwise average $\log_{10}$ population density, precipitation and temperature for province pairs, adjusted for geographical distance between pairs:

$$\hat{\rho}_p = C + \beta_1 d_p + \beta_2 \bar{t}_p + \beta_3 \bar{\kappa}_p + \beta_4 \overline{\log_{10}(\lambda)}_p, \quad \text{[S11]}$$

where ρ is the synchrony of multiannual or annual cycles or the unfiltered IRs between unique province pair p, d is geographical distance in kilometers, t is temperature in degrees Celsius, κ is precipitation in millimeters, and λ is population density per kilometer^2.

1.7. Wavelet Coherency. As an alternative metric for synchrony over time and for comparison with the wave correlation analysis, we measured wavelet coherency between province pairs. As previously described, wavelet coherency uses wave transforms of two time series to indicate their localized phase relationship in a time–frequency spectrum (7, 32). Wavelet coherency ranges from zero to one, and high wavelet coherency requires that statistically significant cycles of a particular periodicity are detected in both time series and that these cycles are phase-dependent (positively or negatively):

$$R_n^2(s) = \frac{\left| S\left(s^{-1} W_n^{XY}(s)\right)\right|^2}{S\left(s^{-1}\left|W_n^X(s)\right|^2\right) \times S\left(s^{-1}\left|W_n^Y(s)\right|^2\right)}, \qquad \textbf{[S12]}$$

where S is a smoothing operator. Statistical significance of wavelet coherency was tested using Monte Carlo methods ($n = 600$) (32). For the wavelet transform in the wave coherency function, we used the same parameters as specified for the wave correlation analysis (i.e., a value for $\omega_0 = 6$ and a δj resulting in a periodicity step size of 1 mo along a linear scale). We only measured wavelet coherency for periodicities below the maximum for each province $s_{max,p}$.

We studied changes over time in wavelet coherency for each province by computing the percentages of other provinces that were statistically significantly coherent with this province at each time point (Fig. S1 *C* and *D*). In addition, we used wavelet coherency to estimate the association between the ONI and the multiannual dengue cycle for each province. For each province, we averaged all statistically significant values of this wavelet coherency matrix within the multiannual periodicity band (19–60 mo).

1.8. Phase Differences. As previously described, we computed phase angles for annual and multiannual cycles as indicators of epidemic timing (2, 30, 31). For each province and for annual and multiannual periodicities separately,

$$\phi_n(s) = \tan^{-1}\left(\frac{\Im\left\{W_n^{XY}(s)\right\}}{\Re\left\{W_n^{XY}(s)\right\}}\right). \qquad \textbf{[S13]}$$

We computed the average phase angle-ϕ_n for annual and multiannual cycles as the circular average of periodicity-specific phase angle-$\phi_n(s)$ across the annual or multiannual periodicity bandwidth (6–18 and 19–60 mo, respectively) as described previously (32). Because we only reconstructed annual and multiannual cycles for provinces with statistically significant cycles in these bandwidths, we only computed phase angles for provinces with statistically significant cycles.

We used these phase angles to compute the phase angle difference θ between provinces for annual and multiannual cycles. The phase angle difference θ was constrained between $-\pi$ and π. We expressed θ in months and assumed a cycle length of 12 mo for annual and 39 mo for multiannual cycles. We used a linear model with a linear spline to measure the relation between θ and geographical distance. We used unique absolute values of θ to only include unique province pairs and included a linear spline to detect the distance after which the relation between θ and distance, d_p, would become nonsignificant:

$$\left|\widehat{\theta_p}\right| = C + \beta_1 d_p + \beta_{p,s=500}^S\left((d_p = s) \times (d_p - s)\right), \qquad \textbf{[S14]}$$

where we varied s with increments of 100 km from a minimum of 500 km up to a maximum S of 2,500 km and selected the best fitting model based on Akake's Information Criterion. The association between θ and distance was only statistically significant before the spline point s. We used the spline point of the best fitting model as the distance radius within which we detected local traveling waves. For multiannual cycles, the s of the best fitting model was at 1,000 km, and for annual cycles, it was at 1,500 km.

1.9. Traveling Waves. We defined a local traveling wave for a province as a statistically significant positive linear association between θ and geographical distances between that province and the other provinces. A province could have a negative or positive θ with other provinces. A negative θ (lag time) indicated that a province was timed later compared to the other province (lagging behind), and a positive θ (lead time) indicated that the province was timed earlier compared to the other province (leading ahead). Outgoing traveling waves can emerge from provinces that are timed ahead of others. Incoming traveling waves can occur for provinces that are timed behind others. For provinces that were lagging behind (negative θ), we defined an incoming traveling wave as a decreasing θ with decreasing distance. For provinces that were leading ahead (positive θ), we defined an outgoing traveling wave as an increasing θ with increasing distance. For each province and separately for annual and multiannual cycles, we used a linear model to detect traveling waves:

$$\theta_{p,q} = \begin{cases} C - \beta_p d_{p,q} & \theta_{p,q} < 0;\ \text{incoming waves for province } p \\ C + \beta_p d_{p,q} & \theta_{p,q} > 0;\ \text{outgoing waves for province } p \end{cases}, \qquad \textbf{[S15]}$$

where p is a province, and q indicates all other provinces. We only included values of d below 1,000 (multiannual cycles) or 1,500 km (annual cycles). We inversed the sign of distance $d_{p,q}$ for $\theta_{p,q}$ values below zero for more intuitive displays of incoming waves (Fig. 5). We tested statistical significance of β_p for incoming and outgoing waves separately for each province. We used Bonferroni-corrected significance levels of 0.0002 per province for a combined significance level of 0.05 for each group of tests: incoming waves of multiannual cycles, outgoing waves of multiannual cycles, incoming waves of annual cycles, and outgoing waves of annual cycles. We measured the association of having multiannual or annual traveling waves (binary variable) for provinces with their average population size, temperature, and precipitation using a logistic regression model. For incoming and outgoing waves of annual and multiannual cycles separately:

$$\tau_p = C + \beta_1 s_p + \beta_2 t_p + \beta_3 \kappa_p, \qquad \textbf{[S16]}$$

where τ_p is a binary variable specifying the presence or not of a traveling wave for a province, s_p is the average population size of a province across study years, t_p is the average monthly temperature in degrees Celsius for a province, and κ_p is the average monthly precipitation in millimeters. Given that we used this model separately for four different waves, we used a Bonferroni-corrected significance level for a combined level of 0.05.

1.10. Sensitivity Analysis. We conducted a sensitivity analysis on the effect of the value for the wavelet parameters ω_0 and δj on synchrony. We computed wavelet transforms as described above for annual and multiannual cycles while varying the value of ω_0 from 2 to 10. For each value of ω_0, we computed the average synchrony between each province and all of the other provinces weighted by the number of pairwise observations (Fig. S6 *A* and *B*). We did the same for values of δj ranging from 0.05 to 0.5 (Fig. S6 *C* and *D*).

1.11. Computing Environment. All analyses were conducted using the R System, version 3.2.1. We used the package dplR for the wavelet analysis with a modified Morlet function with a linear periodicity scale. We used the package biwavelet for wavelet coherency with modified wtc and wt functions with a linear periodicity scale. We used the function Sncf for the nonparametric analysis of the correlation between synchrony and geographical distance.

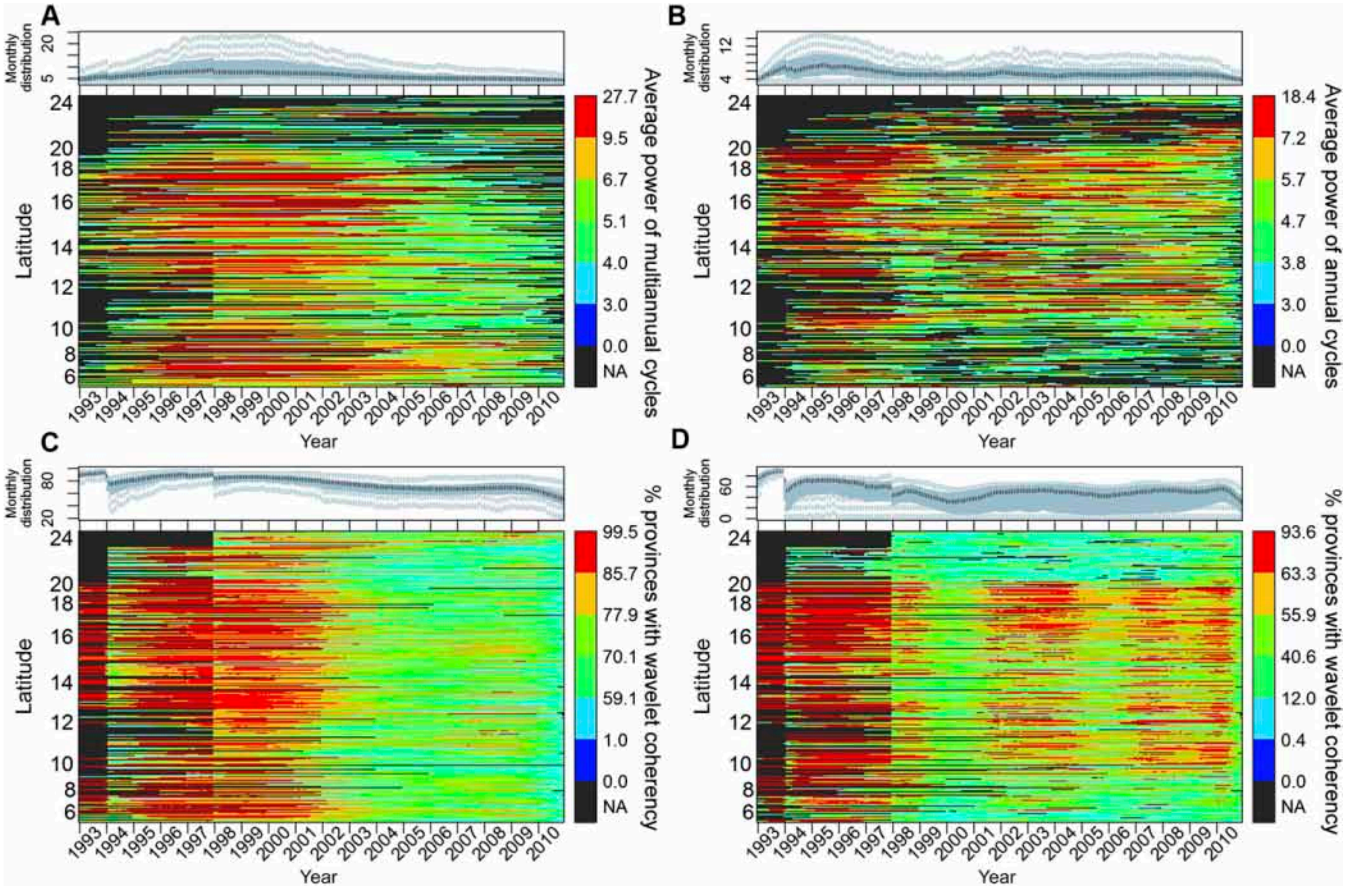

Fig. S1. Changes in periodicity over time in months as shown by wavelet transforms and wavelet coherency. For each province, we computed the average power of statistically significant wavelet transforms per month in the multiannual or annual periodicity band. We also computed for each province the percentage of other provinces that had statistically significant wavelet coherency with this province. *Upper* shows monthly distributions. NA, not available. (*A*) Average power of statistically significant wavelet transforms in the multiannual periodicity band per month for each province ranked by latitude. (*B*) The same as *A* but for the annual periodicity band. (*C*) For each province ranked by latitude, the percentage of other provinces that had statistically significant wavelet coherency with this province for periodicities within the multiannual band. (*D*) The same as *C* but for the annual periodicity band.

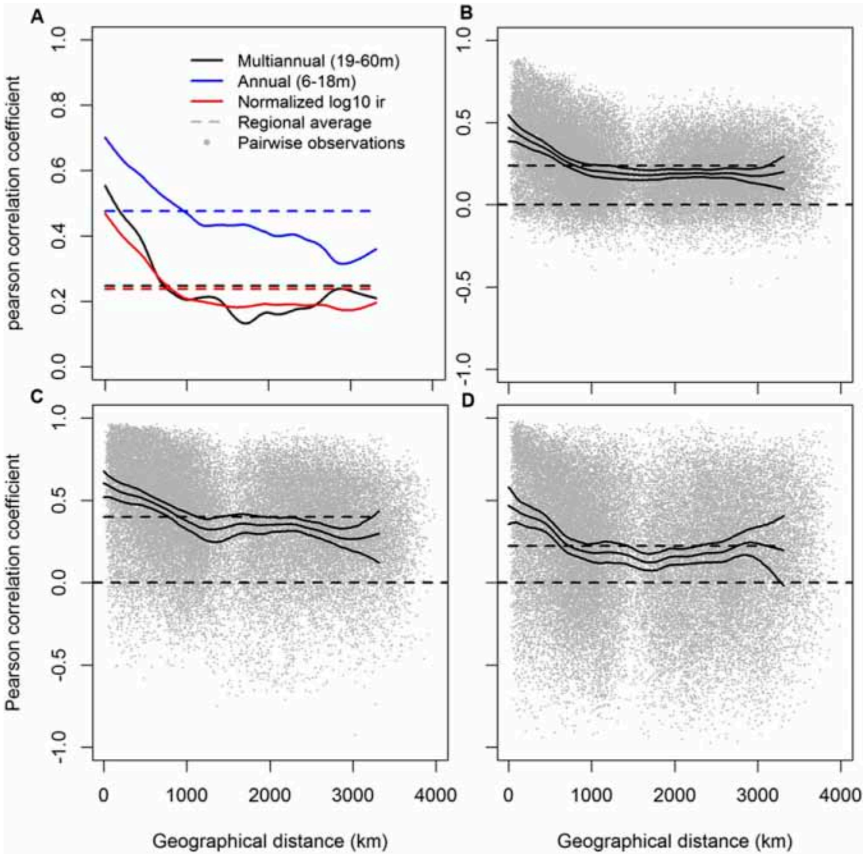

Fig. S2. Cross-correlation function of geographical distance vs. pairwise Pearson correlation. (*A*) Average cross-correlation functions (solid lines) and regional averages (dashed lines) of annual and multiannual cycles and $\log_{10}$ IRs centered and reduced to *z* scores. (*B*) Average cross-correlations and 95% CIs (solid lines) and the regional averages (dashed lines) for $\log_{10}$ IRs centered and reduced to *z* scores. (*C*) The same as *B* but for annual dengue cycles (6–18 mo). (*D*) The same as *B* but for multiannual dengue cycles (19–60 mo).

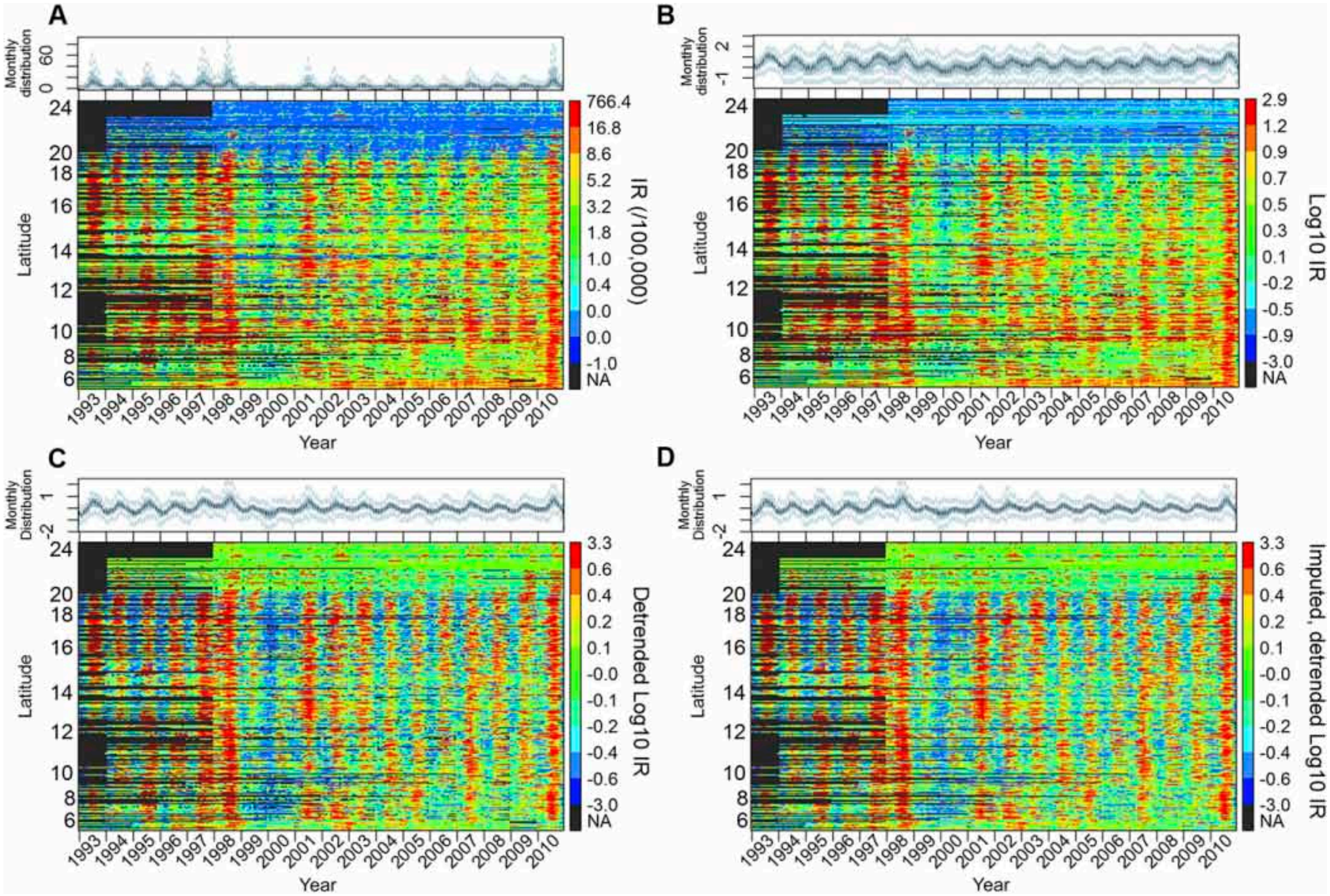

Fig. S3. Dengue IRs and transformations. Monthly values for each province ranked by latitude in color coding. NA, not available. The distributions across provinces per month are shown in *Upper*. (*A*) Reported dengue IRs per 100,000 people. (*B*) Log_{10}-transformed IRs. (*C*) Log_{10}-transformed IRs that were detrended by subtracting fitted values of a linear model. (*D*) The same as in *C* but with missing data imputed.

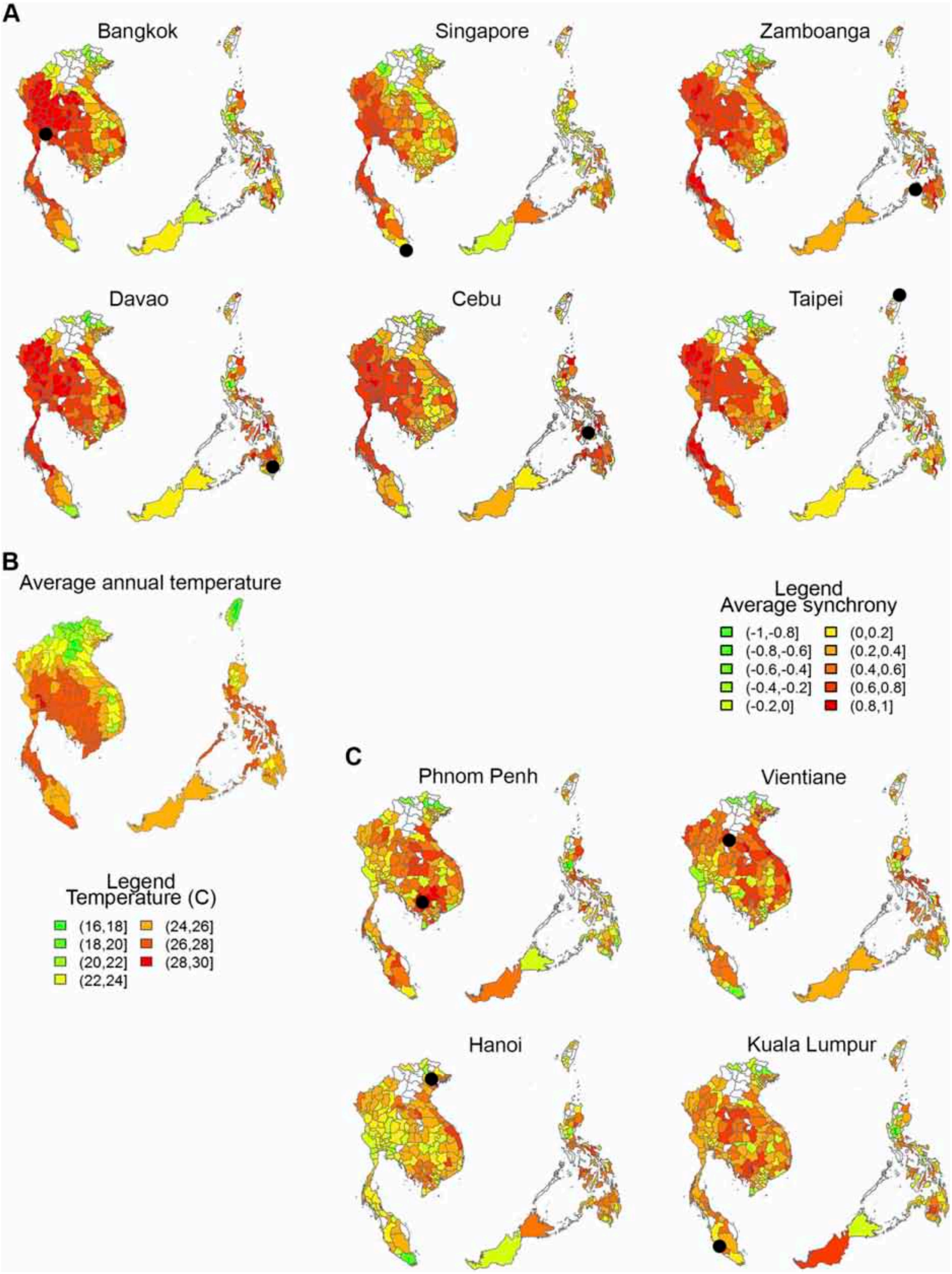

Fig. S4. Average synchrony of multiannual dengue cycles between each of 10 major cities and all other provinces across the entire study period. We found two clusters of cities with different synchrony dependent on temperature. (*A*) Average synchrony of multiannual dengue cycles per province for cities that were not synchronous with the Annamite region. Two of the largest metropolitan areas, Manila and Ho Chi Minh City, had relatively low synchrony with most of the other provinces in the region, including the Annamite region, and are not shown. (*B*) Average annual temperature per province in degrees Celsius. (*C*) Average synchrony of multiannual dengue cycles per province for cities synchronous with the Annamite region.

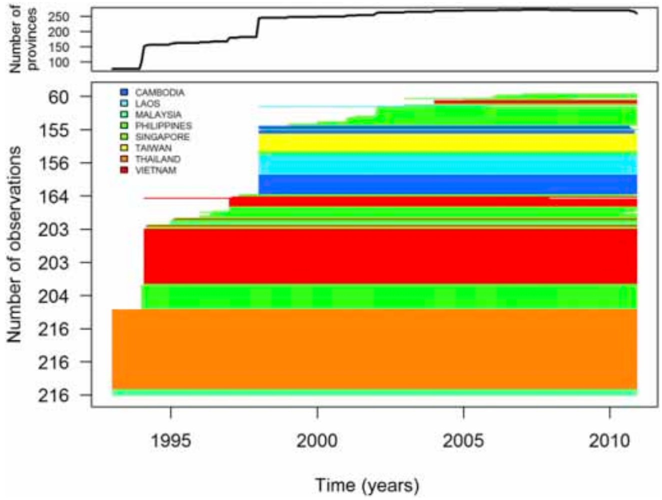

Fig. S5. Monthly data available by province ranked by country. For each province, the months between 1993 and 2010 were included in the analysis for a total of 273 provinces. *Upper* shows the total number of provinces included per month. The length of the time series determined the maximum periodic cycle that could be studied by wavelet analysis. To reduce edge effects, we defined the maximum periodicity for each province as the number of observations divided by 2.5 (i.e., the time series should be able to contain at least 2.5 repeats of a periodic cycle).

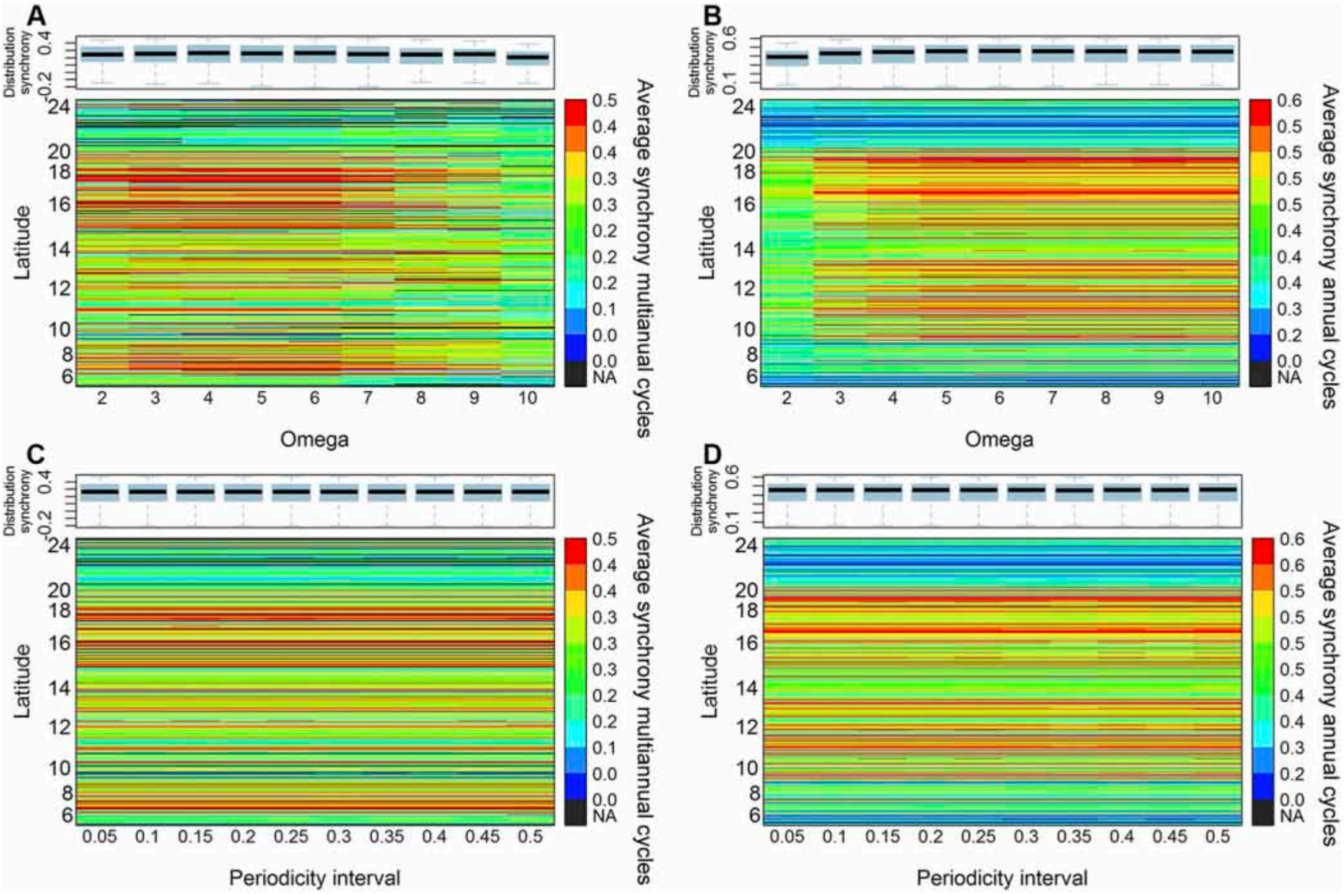

Fig. S6. Sensitivity analysis of average synchrony per province for different values of ω_0 and δj. We reconstructed multiannual and annual cycles using different values for the wavelet parameters ω_0 and δj and recomputed the average correlation coefficient per province weighted by the number of province pairs with non-missing data. We used an ω_0 of 6 and a δj of 0.25 in our analysis. NA, not available. (*A*) Average synchrony of multiannual cycles for values of ω_0. (*B*) The same as *A* for annual cycles. (*C*) Average synchrony of multiannual cycles for values of δj. (*D*) The same as *C* for annual cycles.

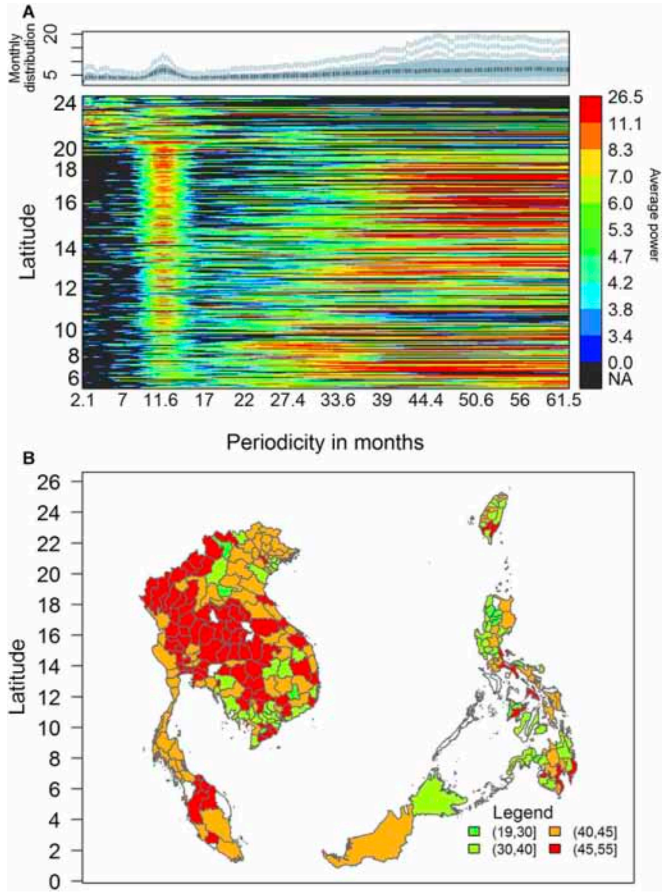

Fig. S7. Variance explained by different periodicities for each province. We used wavelet analysis for periodicities ranging from 2 mo to the maximum periodicity for a province, with a 1-mo step size along a linear scale. (*A*) The global wavelet power spectrum using only statistically significant wavelet transforms per province ranked by latitude. *Upper* shows the distributions across provinces. NA, not available. (*B*) The average multiannual periodicity across periodicities ranging from 19 to the maximum supported by a province time series weighted by the average power for each periodicity.

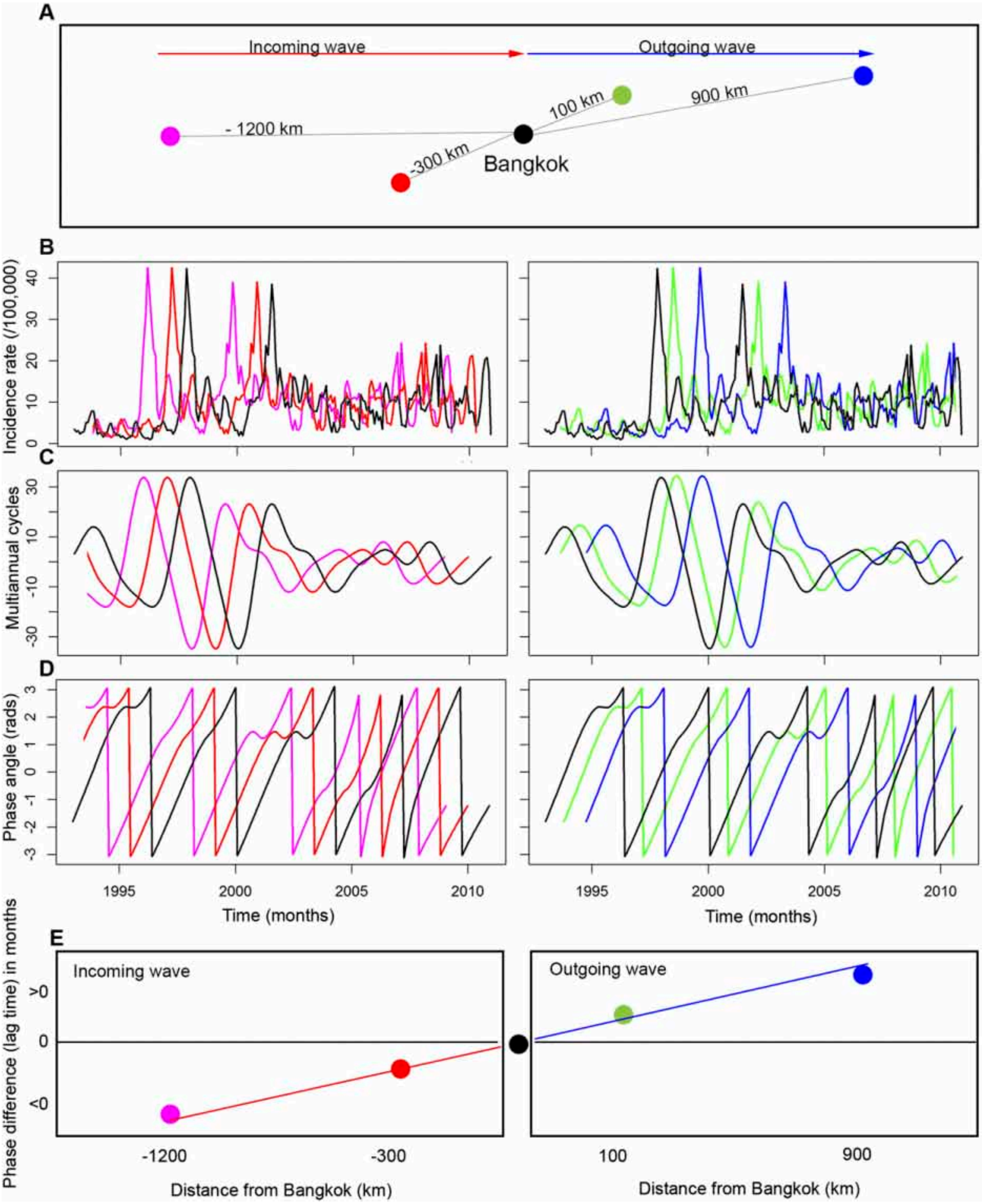

Fig. S8. Local traveling waves for Bangkok and four hypothetical example provinces. (*A*) Location of Bangkok and four hypothetical provinces at varying distances. (*B*) IRs (per 100,000 people) for each location. (*C*) Wavelet reconstruction of multiannual (19–60 m) dengue cycles. (*D*) Phase angles of multiannual dengue cycles. (*E*) Linear model fit of the association between lag time in months and geographical distance from Bangkok. For negative phase angle differences, we inversed the geographical distance for a more intuitive display. Incoming traveling waves into Bangkok were defined as decreasing lag times with decreasing distance (other provinces timed ahead of Bangkok). Outgoing waves emerging from Bangkok were defined as increasing lag times with increasing geographical distance (other provinces timed after Bangkok). We measured the presence of these incoming or outgoing traveling waves for each province in our study (Fig. 5).

Table S1. Linear models of annual and multiannual synchrony vs. climate and population covariates

Periodicity and covariate	Coefficient (95% CI)	*P* value
Annual*		
Distance (100 km)	−0.006 (−0.007 to −0.006)	<0.00001
Temperature (°C)	0.004 (0.002 to 0.005)	0.0002
Precipitation (cm)	−0.012 (−0.013 to −0.012)	<0.00001
Log_{10} population density (population per 1 km^2)	−0.088 (−0.095 to −0.081)	<0.00001
Multiannual†		
Distance (100 km)	−0.006 (−0.007 to −0.006)	<0.00001
Temperature (°C)	0.029 (0.026 to 0.031)	<0.00001
Precipitation (cm)	0.001 (0.000 to 0.002)	0.0079
Log_{10} population density (population per 1 km^2)	−0.037 (−0.047 to −0.028)	<0.00001

For each province pair, we regressed synchrony vs. the pairwise average of each covariate, except for distance.
*$R^2 = 0.14$.
†$R^2 = 0.06$.

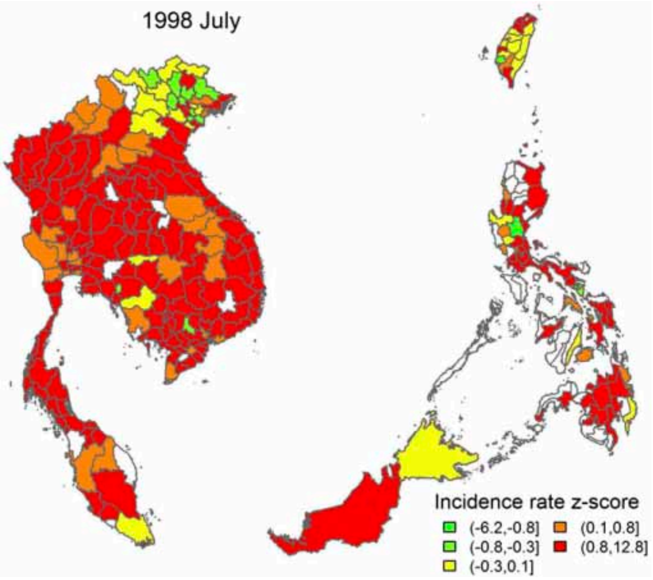

Movie S1. Monthly IRs (per 100,000 people) were $\log_{10}$-transformed and detrended, and missing values were imputed. For each province, IRs were then centered and reduced (normalized) to *z* scores (SDs from the mean) to increase cross-province comparability. This movie shows maps of these *z* scores for each month in the 1993–2010 time series.

Movie S1